frontiers in Earth Science

ORIGINAL RESEARCH
published: 28 February 2018
doi: 10.3389/feart.2018.00016

Distinguishing Biologically Controlled Calcareous Biomineralization in Fossil Organisms Using Electron Backscatter Diffraction (EBSD)

Jan-Filip Päßler†, Emilia Jarochowska, Michel Bestmann and Axel Munnecke*

GeoZentrum Nordbayern, Friedrich-Alexander-Universität Erlangen-Nürnberg, Erlangen, Germany

Although carbonate-precipitating cyanobacteria are ubiquitous in aquatic ecosystems today, the criteria used to identify them in the geological record are subjective and rarely testable. Differences in the mode of biomineralization between cyanobacteria and eukaryotes, i.e., biologically induced calcification (BIM) vs. biologically controlled calcification (BCM), result in different crystallographic structures which might be used as a criterion to test cyanobacterial affinities. Cyanobacteria are often used as a "wastebasket taxon," to which various microfossils are assigned. The lack of a testable criterion for the identification of cyanobacteria may bias their fossil record severely. We employed electron backscatter diffraction (EBSD) to investigate the structure of calcareous skeletons in two microproblematica widespread in Palaeozoic marine ecosystems: *Rothpletzella*, hypothesized to be a cyanobacterium, and an *incertae sedis* microorganism *Allonema*. We used a calcareous trilobite shell as a BCM reference. The mineralized structure of *Allonema* has a simple single-layered structure of acicular crystals perpendicular to the surface of the organism. The *c*-axes of these crystals are parallel to the elongation and thereby normal to the surface of the organism. EBSD pole figures and misorientation axes distribution reveal a fiber texture around the *c*-axis with a small degree of variation (up to 30°), indicating a highly ordered structure. A comparable pattern was found in the trilobite shell. This structure allows excluding biologically induced mineralization as the mechanism of shell formation in *Allonema*. In *Rothpletzella*, the *c*-axes of the microcrystalline sheath show a broader clustering compared to *Allonema*, but still reveal crystals tending to be perpendicular to the surface of the organism. The misorientation axes of adjacent crystals show an approximately random distribution. *Rothpletzella* also shares morphological similarities with extant cyanobacteria. We propose that the occurrence of a strong misorientation relationship between adjacent crystals with misorientation axes clustering around the *c*-axis can be used as a proxy for the degree of control exerted by an organism on its mineralized structures. Therefore, precisely constrained distributions of misorientations (misorientation angle and misorientation axis) may be used to identify BCM in otherwise problematic fossils and can be used to ground-truth the cyanobacterial affinities commonly proposed for problematic extinct organisms.

Keywords: biomineralization, cyanobacteria, fossil, microproblematica, EBSD, crystallography, carbonate

OPEN ACCESS

Edited by:
Karim Benzerara, Centre National de la Recherche Scientifique (CNRS), France

Reviewed by:
Daniel Vielzeuf, UMR7325 Centre Interdisciplinaire de Nanoscience de Marseille (CINaM), France
Jarosław Stolarski, Institute of Paleobiology (PAN), Poland

****Correspondence:***
Emilia Jarochowska
emilia.jarochowska@fau.de

†Present Address:
Jan-Filip Päßler, Department of Palaeontology, University of Vienna, Vienna, Austria

Specialty section:
This article was submitted to Biogeoscience, a section of the journal Frontiers in Earth Science

Received: *29 September 2017*
Accepted: *14 February 2018*
Published: *28 February 2018*

Citation:
Päßler J-F, Jarochowska E, Bestmann M and Munnecke A (2018) Distinguishing Biologically Controlled Calcareous Biomineralization in Fossil Organisms Using Electron Backscatter Diffraction (EBSD). Front. Earth Sci. 6:16. doi: 10.3389/feart.2018.00016

INTRODUCTION

Types of Biomineralization

Biomineralization refers to the process of formation of mineral phases carried out by organisms. It can occur in two fundamentally different ways, depending on the degree of biological control over the formation (Lowenstam, 1981; Weiner and Dove, 2003). The first is biologically controlled mineralization (BCM), in which organisms have extensive control over the mineral formation. BCM results in well-ordered mineral structures with minor size variations and species-specific crystal habits (Bazylinski and Frankel, 2003). The second is biologically induced mineralization (BIM), in which organisms have no to minor control over the mineral formation. BIM results in heterogeneous mineral compositions with poor crystallinity, including large size variations, poorly defined crystal morphologies and the inclusion of impurities (Banfield and Hamers, 1997; Frankel and Bazylinski, 2003; Weiner and Dove, 2003). It is most typical but not limited to the extracellular calcareous structures formed by cyanobacteria (Lowenstam, 1986; Obst et al., 2009). Finally, structures indistinguishable from BIM products can be also produced in the absence of organisms and highly organized minerals may form in the presence of organic abiotic substrates (e.g., Gower and Tirrell, 1998; Bosak et al., 2004; Benzerara et al., 2010; Oppenheimer-Shaanan et al., 2016). The range of crystallographic properties of biologically and abiotically induced calcitic structures largely overlap and there is currently no criterion allowing their distinction.

Identification of Calcareous Cyanobacteria in the Fossil Record

In the Phanerozoic, biomineralization is widespread in many clades of protists, plants, and animals (Knoll, 2003), but in the early Earth history cyanobacteria were the first organisms capable of calcification, and this capability presumably had a fundamental impact on the ecosphere (Arp et al., 2001; Riding, 2006). It was not only sufficient for rock formation, but also transformed the global carbon cycle (Van Cappellen, 2003; Altermann et al., 2006). Cyanobacteria and/or chloroplasts, their descendants, are responsible for transferring most of the inorganic carbon that enters the biosphere from the inorganic to organic reservoir (Lochte and Turley, 1988). The oldest known cyanobacteria are reported from Paleoarchean (3.3–3.5 Ga) carbonaceous cherts (Schopf and Packer, 1987). However, the first evidence of calcified cyanobacteria only dates back to 750–700 Ma (Swett and Knoll, 1985). Based on a compilation of fossil reports of cyanobacteria, Riding (2006) proposed that CO_2 concentrating mechanisms, essential in cyanobacterial BIM, developed during the Neoproterozoic, and calcified cyanobacteria only became widespread around the early Cambrian (ca. 580 Ma; Riding and Voronova, 1984). Many forms of problematic microfossils are only known from their calcareous shells or sheaths and, based on their morphology, interpreted as cyanobacteria (Flügel, 2004; Vachard and Cózar, 2010). These structures are given Latin names and placed in complex classification systems, but often they are extremely variable morphologically and nearly featureless, resulting in a substantial volatility of their proposed phylogenetic positions (Wray, 1977; Riding and Voronova, 1984; Riding, 2011). Cyanobacteria thus serve commonly as a "wastebasket taxon." Palaeontologists tend to "dismiss" microfossils as cyanobacteria whenever their morphology and shell structure does not correspond to any well understood group. This approach is likely to result in a failure to discover yet unknown fossil groups. It may distort our understanding of cyanobacterial evolution and its impact on global ecosystems. In the fossil record, calcareous structures are commonly the only remnants of problematic organisms and thus the only sources of potential information on their taxonomic affinities. The identification of consistent criteria distinguishing BCM and BIM/abiotic products would permit distinguishing biomineralizing animals and clarifying the position of a large number of calcareous organisms putatively considered to be cyanobacteria.

Principles of Electron Backscatter Diffraction (EBSD)

EBSD is a high-energy electron-beam technique based on elastic scattering of a focused electron beam on a high polished surface. Penetrating the sample, some electrons are backscattered through the lattice planes of an examined crystal, satisfying the Bragg condition of diffraction. The result is two cones of backscattered electrons with a mirror plane in between which equals one Kikuchi Line. Multiple Kikuchi lines are described as Kikuchi pattern, representing all lattice planes of a crystal with its specific orientation in a 2D projection. These patterns can be automatically indexed by the acquisition software resulting in complete 3D crystal orientations with a high spatial resolution. The crystallographic orientation of each measuring point of a scanned area will be color coded with respect to their Euler angles (mathematic operations which transfer/rotate the crystal coordinate system into the sample coordinate system) and will be presented in so-called orientation maps. For a more detailed description about the method, see Prior et al. (1999). For a discussion of applications to biological specimens, see e.g., Griesshaber et al. (2010) and Cusack (2016).

Aims of the Study

Calcareous microproblematica are widespread in Palaeozoic carbonate deposits, functioning as reef builders, primary producers, and as key components of many carbonate factories. Here we address two common examples of them, *Allonema* and *Rothpletzella* (Wood, 1948; Flügel, 2004; Nose et al., 2006; Jarochowska and Munnecke, 2014). It is striking that the affinity and biology of these organisms remain essentially obscure (Wilson and Taylor, 2001; Jarochowska and Munnecke, 2014), excluding them from ecological and macroevolutionary analyses. The aim of this study is to test whether the crystallography of the calcareous mineralized structures of fossil microproblematica can aid in the identification of their mode of biomineralization and, consequently, in constraining their affinity. To this aim, we employ electron backscatter diffraction (EBSD) analysis of the calcareous walls of these organisms.

MATERIALS AND METHODS

Calcareous Microproblematica

Allonema

Allonema (Ulrich and Bassler, 1904; **Figures 1A,B**), is a microscopic epibiont commonly found in Palaeozoic (Ordovician to Carboniferous) marine carbonates. It is composed of irregularly arranged, branching tubes forming clearly separated vesicles with diameters around 100 μm (Jarochowska and Munnecke, 2014). The wall or mineralized structure of the organism is calcareous, punctate and, with respect to the whole organism, very thin, making up about 15% of the width of the body (Jarochowska et al., 2016). The shape of a single vesicle is hemispheric to lunate (Riding, 1977b). The phylogenetic position of *Allonema* is controversial and underwent many revisions since it was tentatively established by Ulrich and Bassler (1904), who classified it as a ctenostome bryozoan. Most recent publications regard *Allonema* as *incertae sedis* (Jarochowska and Munnecke, 2014; Wilson and Taylor, 2014; Liu et al., 2016).

Rothpletzella

Rothpletzella (Wood, 1948; **Figures 1C,D**), is a problematic organism commonly found in Palaeozoic (Early Ordovician to Late Devonian) marine carbonates (Wood, 1948). It is composed of irregularly arranged, tube-like threads with diameters between 30 and 35 μm. The tubes are non-septate and appear as a "string of pearls" in oblique sections. Branching dichotomously in one plane is very common (Flügel, 2004). *Rothpletzella* commonly co-occurs with *Allonema* (Liu et al., 2016; Zhang et al., 2017). Both are common in Palaeozoic back-reef, fore-reef, as well as open-marine and semi-restricted shelf limestones, where they play an important role in the formation of oncoids and mounds of microbial origin (e.g., Shen and Neuweiler, 2016). As in the case with *Allonema*, the taxonomical classification of *Rothpletzella* is unclear. Although a cyanobacterial affinity is proposed by a few authors (Jarochowska and Munnecke, 2014), *Rothpletzella* is often regarded as *incertae sedis* (Riding, 1991; Liu et al., 2016).

Sample Information

Three sets of samples from the Silurian of Gotland, Sweden, were used for this study. The first is from the Tofta Formation, Sheinwoodian (mid-Silurian, ca. 430 Ma) located at the abandoned quarry of Nors Stenbrott (λ N 57°51′51.78″, ϕ E 18°41′04.48″). The second set is taken from the Mulde Brick-clay Member of the Homerian (mid-Silurian, ca. 427 Ma) Halla Formation at the locality Blåhäll 1 in the west of Gotland (λ N 57°18′44.65″, ϕ E 18°09′19.79″). The third set is taken from the Eke Formation, Ludlow (late Silurian, ca. 423 Ma) from an outcrop at Lau Backar, South-East of Gotland (approx. 1,250 m ENE from the church at the village of Lau; λ N 57°17′15.25″, ϕ E 18°38′28.78″).

Sample Preparation

All samples were cut parallel to the direction of growth of organisms. Three thin sections and two polished blocks were produced. They were pre-polished mechanically with 9 and 3 μm diamond suspension and subsequently chemically-mechanically polished with SYTON (Köstrosol 3530) for 4 h, and coated with a 3.4–3.8 nm layer of carbon.

EBSD Data Acquisition

EBSD mapping was performed at the GeoZentrum Nordbayern, using a TESCAN Vega II (tungsten filament) SEM equipped with an Oxford Instrument EBSD system including a Nordlys-II S EBSD camera and Channel5 acquisition software. Working conditions were: 30 kV acceleration voltage, beam current between 1.1 and 1.2 nA and 20 mm working distance. The center and sometimes the edges of 6–7 Kikuchi bands were automatically detected using the Hough transform routine with a resolution of 85 (i.e., internal Hough resolution parameter in the software). The solid angle calculated from the patterns was compared with a calcite match unit containing 75 reflectors. All maps were scanned with a 0.3 μm step size. The threshold parameter MAD (mean angular deviation between the detected Kikuchi bands and the simulation) for confident pattern indexing was set to <1.2.

EBSD Data Display and Processing

Interpreting EBSD Data

EBSD data are presented as processed orientation maps, in which each pixel represents one data point. The color of each pixel depends on the superposition of three color channels (red, green and blue) which are assigned to the values of the three Euler angles measured for each point. Non-indexed points were replaced by the most common neighbor orientation. The degree of processing required in order to fill non-indexed data points, without introducing artifacts, was tested carefully by comparison of the resulting orientation map with the pattern quality mapping (Bestmann and Prior, 2003). The criterion for defining a new crystal surrounded by high-angle grain boundaries was based on misorientation axis analysis. Following Maier et al. (2014), the critical misorientation angle was set to 30°. However, for our study, cross-checking revealed that for all analyzed organisms a threshold of 15° separates adjacent orientation domains. These domains are also discriminated by changes in color coding in the orientation maps, even when for some organisms (here represented by *Allonema*) misorientation axis analysis exhibits pronounced clustering around a specific crystallographic direction (i.e., *c*-axis) for misorientation angles $>30°$ (see section *Allonema*). Therefore, high angle boundaries ($>15°$) are marked with black lines in the orientation maps. Based on the orientation maps, the mineralized structures of the organisms were subdivided into several approximately homogeneous subsets. The crystallographic orientations (*c*- and *a*-axis) of these subsets are presented as pole figures (PFs—equal area upper hemisphere plots). In addition, $+a$ and $-a$ axes are discriminated by plotting the data in the upper and lower hemisphere. The colors of data points shown in PFs (sample coordinate system) equal the colors of the orientation maps.

Distribution of Misorientation Axes

Orientation maps constructed from EBSD have an enormous potential in microstructural studies because different

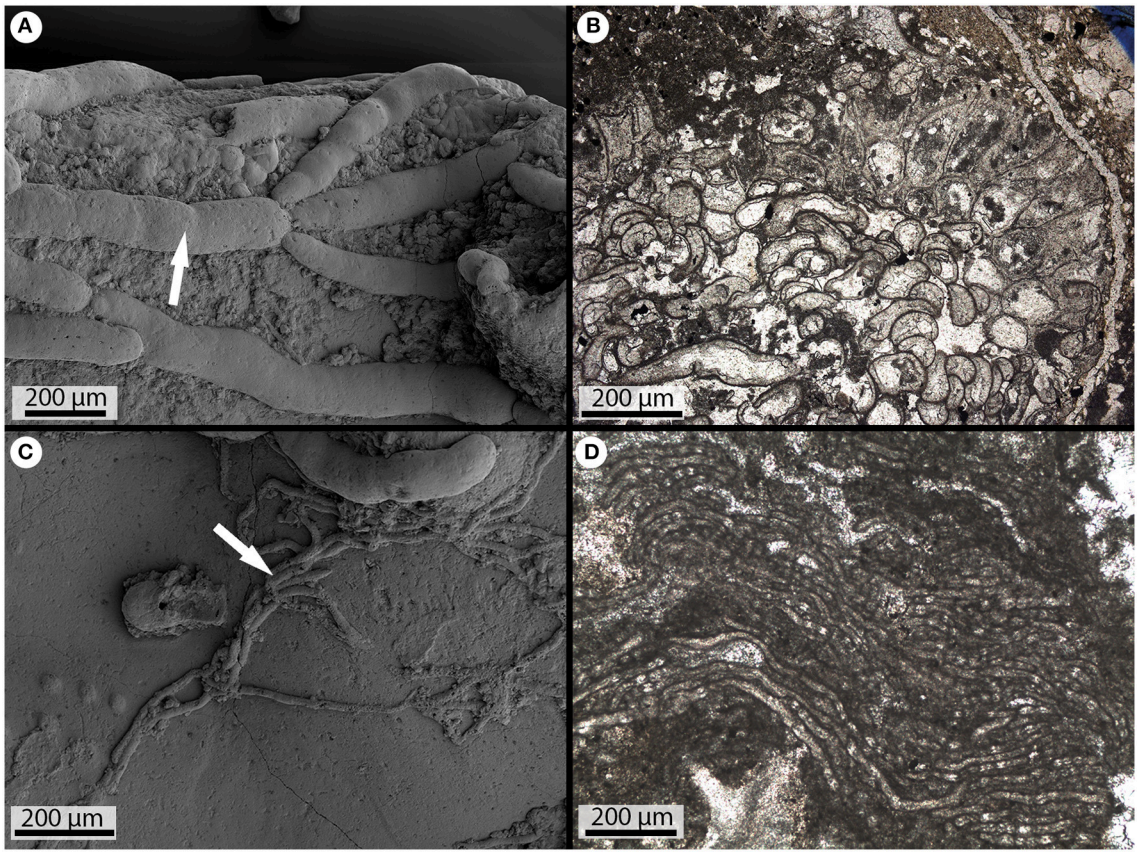

FIGURE 1 | Fossil calcareous microproblematica. **(A)** SEM picture of an *Allonema* colony (arrow) in its 3D aspect (Silurian of Gotland). **(B)** Thin section of an *Allonema* colony in its 2D aspect (Ordovician of Canada). **(C)** SEM picture of *Rothpletzella* in its 3D aspect (Silurian of Gotland). **(D)** Thin section of multiple *Rothpletzella* tubes (Silurian of Gotland).

models of microstructural development predict particular relationships between adjacent grains (e.g., Gilbert et al., 2008; Coppersmith et al., 2009; Floquet and Vielzeuf, 2011). Analysis of misorientation distributions is a powerful tool to quantify microstructural features (e.g., Prior et al., 2002 and references within). The misorientation between two lattices can be expressed by a rotation axis and rotation angle. By definition the minimum misorientation angle and its corresponding axis from all possible symmetric variants is used (e.g., Wheeler et al., 2001). Misorientation axes of low (2–15°) and high (>15°) misorientation angle boundaries are presented as inverse pole figures (IPFs) with respect to the crystal coordinate system (equal area upper hemisphere plots). The misorientation axes are plotted with a misorientation angle up to 75° since no misorientations of higher angles appeared, whereas the theoretical maximum misorientation angle for the trigonal crystal symmetry of calcite is 104° (Wheeler et al., 2001).

RESULTS

Allonema

Seven EBSD scans containing *Allonema* vesicles were performed on three samples. These scans comprise oblique to longitudinal sections through vesicles of multiple individuals. The vesicles have various shapes described as hemispheric to lunate. The heights of these vesicles vary between 50 and 170 µm. The lengths range from 100 to 640 µm. The thickness of the walls or mineralized structures of single vesicles is relatively homogeneous throughout one specimen. The thicknesses of the upper vesicle walls (e.g., **Figure 2A**) vary between 10 and 60 µm and the bottom walls are approximately half as thick as the upper walls.

Crystals comprised within the upper walls have lengths between 10 and 50 µm and diameters that range from 2 to 5 µm. Crystals forming the bottom walls are much smaller (5–15 µm in length and <1 to 2 µm in diameter). The morphologies of the crystals defining the mineralized structures are described as elongated granular (smaller crystals) to acicular (larger crystals—**Figure 2A**).

The subsets defined for *Allonema* reveal a single maximum of *c*-axes <0001> indicating a strictly parallel orientation around the *c*-axis of adjacent crystals within each subset. The orientation maximum rotates continuously with respect to the curvature of the vesicle (**Figures 2A,B**). The PFs of elongated granular and acicular crystals indicate that their *c*-axes are parallel to the elongation of the crystals, thus they are perpendicular to the

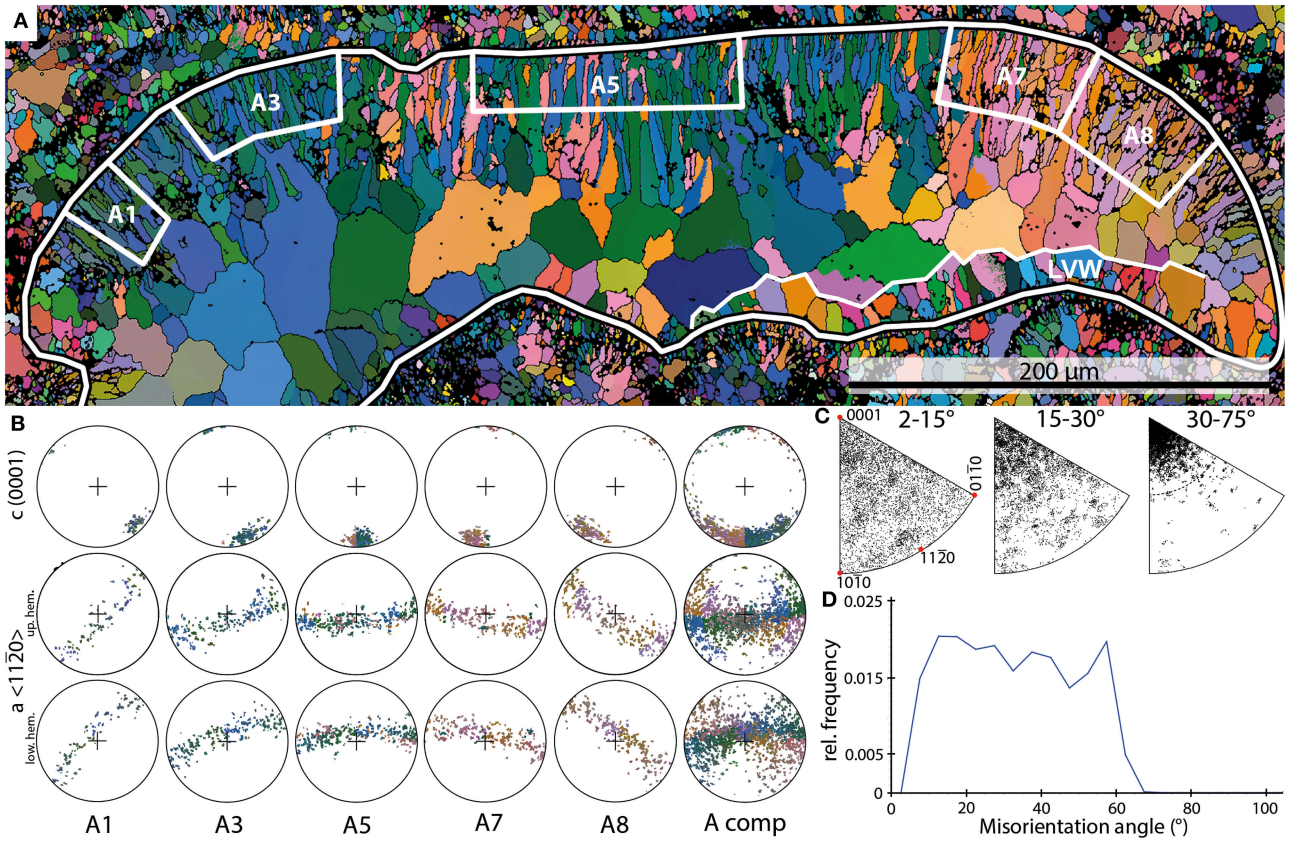

FIGURE 2 | Examples of the results of EBSD scans on *Allonema*. **(A)** EBSD orientation map of an *Allonema* vesicle shown in cross section (black-white outline); white boxes A1 through A8 mark subsets of the upper vesicle wall shown in **(B)**. LVW—lower vesicle wall. **(B)** Pole figures (PFs) of the subsets marked in **(A)** and the entire shell of the vesicle (A comp). **(C)** Inverse PFs (IPFs) of misorientation axes measured for the entire shell without the large sparite crystals within the vesicle. **(D)** Misorientation angle distribution of *Allonema* shell crystals.

surface of the vesicles (**Figures 2A,B**). The *a*-axes <11–20> are parallel to the surface of the vesicles for each subset and reveal a girdle distribution indicating a fiber-texture around the *c*-axis.

The IPF plots of misorientation axes between adjacent crystals (**Figure 2C**) reveal a broad scattering for low misorientation angles (2–15°). For angles between 15 and 30°, a weak clustering toward the *c*-axis is recognizable, nevertheless misorientation angles are still scattered broadly. When even higher angle boundaries (30–75°) are considered, a strong clustering around the crystallographic *c*-axis is evident with a scattering angle up to 25–30°.

Thus, these clusters support the idea of a highly ordered, parallel arrangement of adjacent crystals with a slight error or "wobbling" up to a maximum of 30° around the *c*-axis. These cluster distributions indicate a smooth transition between the crystals throughout the mineralized structure of a single *Allonema* vesicle.

The frequency distribution of misorientation angles (**Figure 2D**) range from 2 to 67° with a steep increase from 2° to the first dominant maximum around 12° and a steep decline from the second dominant maximum around 57° to a minimum at 67°. The relative frequencies between both maxima show a slight decline. The overall distribution can be described as trapezoid-shaped.

The crystals defining the bottom walls are poorly preserved. Thus, they could not be measured consistently. In parts with a good preservation of small acicular crystals, the PFs indicate that the *c*-axes are perpendicular to the surface of the vesicle. IPFs of misorientation axes indicate rotations around the *c*-axis similar to the observations of the upper wall structure. However, rotations around the normal to the *m*-plane and *a*-axis are common, indicating a lower degree of order of the crystals as described for the upper walls.

Rothpletzella

Four EBSD scans of *Rothpletzella* vesicles were performed on one sample. These scans comprise cross- and oblique sections through multiple vesicles. The shape of the vesicles is spherical to elliptical. The vesicles have diameters between 45 and 65 µm with a wall thickness between 5 and 10 µm, corresponding to the thickness of the areas R1 through R3 in **Figure 3**.

The wall of individual vesicles is composed of small, granular to elongated crystals. These crystals range from 1 to 10 µm. The crystals defining the walls of *Rothpletzella* vesicles form a smooth

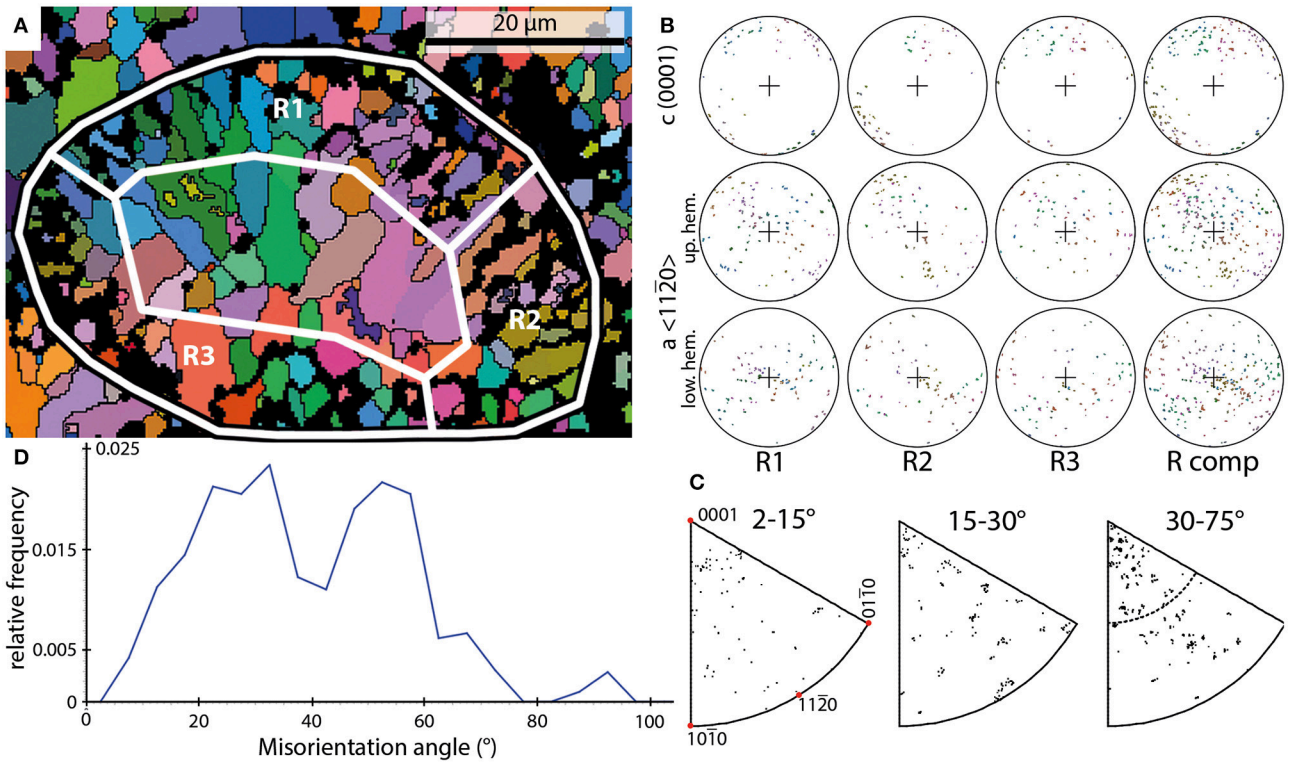

FIGURE 3 | Examples of the results of EBSD scans on *Rothpletzella*. **(A)** EBSD orientation map of a *Rothpletzella* vesicle shown in cross section (black-white outline); white boxes mark subsets shown in **(B)** and span the entire wall thickness. **(B)** PFs of the subsets marked in **(A)** and the entire shell (R comp). **(C)** IPFs of misorientation axes measured for the entire shell without the sparite crystals within. **(D)** Misorientation angle distribution of *Rothpletzella* wall-structure.

surface all around the vesicles. No crystal penetrates this specific line toward the outside and inside of a vesicle (**Figure 3A**). The crystal orientations of *Rothpletzella* walls could be only partly measured, particularly for crystals below 1 µm.

In contrast to the observations made for *Allonema*, the crystals of *Rothpletzella* commonly reveal a strong dispersion within the PFs. The *c*-axes show a scattering along the periphery of the PFs but also dispersion toward the middle of the PFs. The *a*-axes build up a broad girdle distribution, defining a fiber-texture with strong dispersion around the *c*-axis. The PFs of elongated crystals indicate that the *c*-axes are parallel to the elongation, thus they are approximately perpendicular to the surface of the vesicles. The color coding in the orientation map (**Figure 3A**) reveals a weak parallel arrangement of adjacent crystals.

The IPFs of misorientation axes across the entire spectrum of the presented misorientation angles (2–75°) between adjacent crystals reveal a nearly random distribution (**Figure 3C**). Thus, the misorientation relationship between adjacent crystals is not defined by a rotation around a specific crystallographic direction.

These observations support the idea of a poorly ordered, weak parallel arrangement of crystals within the mineralized structures of *Rothpletzella* vesicles.

The frequency distribution of misorientation angles (**Figure 3D**) range from 2 to 77° with two dominant maxima around 32 and 52°. Between these maxima a strong decline of relative frequencies has its lowest point around 42°. The overall distribution can be described as bimodal asymmetric.

Trilobite

Three EBSD scans of trilobite fragments were performed on two samples. These scans comprise cross sections through segments most likely belonging to a pleural lobe (**Figure 4A**). Characteristically for trilobite exoskeletons, they show a continuous undulating extinction under crossed polarizers.

The size of the crystals within the fragments ranges from 1 to 20 µm. The crystals appear in the orientation map as an interconnection of mainly two orientation domains with an irregular patchy appearance and with lobate grain boundaries (**Figure 4B**).

The individual *c*-axis plots of three subsets (T1–T3; **Figures 4B,C**) show pronounced single maxima which together define a smooth dispersion path (Tcomp; **Figure 4C**). The *a*-axis builds a girdle distribution perpendicular to the *c*-axis maximum. The orientation map (**Figure 4B**) in combination with misorientation axis plots (**Figure 4D**) reveal a strong orientation relationship between two adjacent orientation domains (T1: red and blue, T2+T3: blue and brown) with misorientation axes subparallel to the *c*-axis.

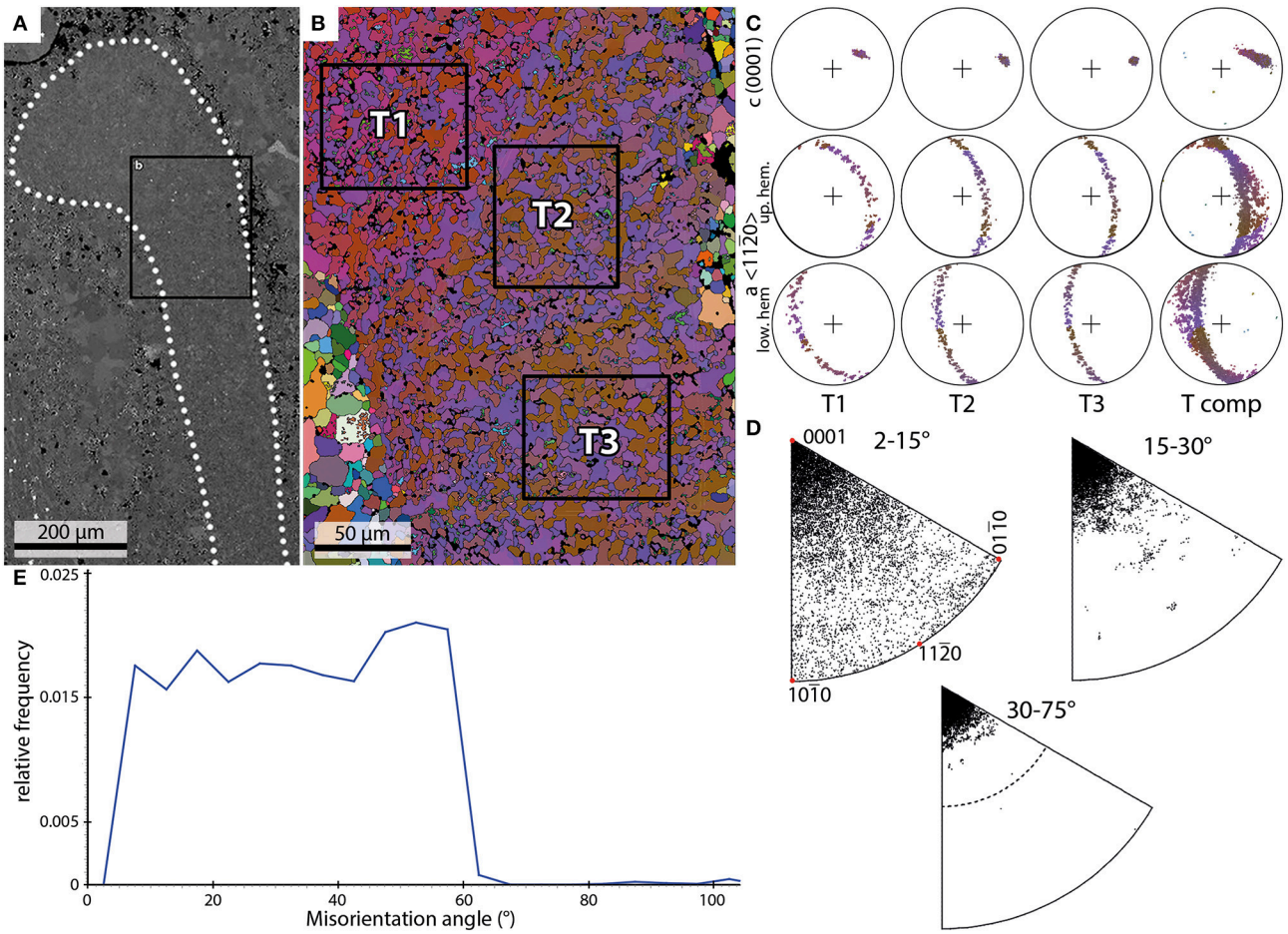

FIGURE 4 | Examples of the results of EBSD scans of a trilobite shell. **(A)** Backscatter image of a trilobite pleural lobe (dotted outline) and the position of the EBSD scan (black box) shown in **(B)**. **(B)** EBSD orientation map; black boxes mark subsets shown in **(C)**. **(C)** PFs of the subsets marked in **(B)** and data from the entire scan (T comp). **(D)** IPFs of misorientation axes measured for the entire shell fragment. **(E)** Misorientation angle distribution of trilobite shell crystals.

The frequency distribution of misorientation angles (**Figure 4E**) range from 2 to 67°. The relative frequencies show a more-or-less homogeneous distribution in range from 5 to 42°. A maximum is observed around 52°. The distribution can be described as nearly trapezoid-shaped.

INTERPRETATION AND DISCUSSION

The wall structures of the examined organisms are characterized by the EBSD data, in particular by the (1) crystal size, (2) crystallographic orientation (i.e., *c*- and *a*-axis), and (3) the crystallographic relationship between neighboring grains (i.e., misorientation angle and misorientation axis).

No EBSD studies have been performed on microbially-produced carbonates so far. Therefore, examined structures were compared with those of extant organisms of known affinity. Proposed affinities for the examined organisms are tested by comparing with descriptions of crystal shapes, orientations, and arrangements documented in the literature.

Rothpletzella

Rothpletzella shows many similarities with extant filamentous cyanobacteria, e.g., the size and shape of crystals in its calcareous sheath (Riding, 1977a; Merz, 1992; Buczynski and Chafetz, 1993; Kazmierczak and Altermann, 2002; Planavsky et al., 2009). A cyanobacterial affinity was proposed for *Rothpletzella* by a few authors (Wood, 1948; Wray, 1977; Nose et al., 2006). Yet recently *Rothpletzella* is regarded as a microproblematicum, since no extant analogs are known (Riding, 1977b, 1991; Liu et al., 2016). The diameters of *Rothpletzella* tubes (25–40 µm) observed in this study fall into the diameter range described for filamentous cyanobacteria (e.g., *Scytonema*, *Phormidium* or *Plectonema*). Contrary to the light microscopy observations by Wood (1948), who described calcite crystals with "haphazard arrangement" within *Rothpletzella* walls, EBSD scans reveal crystal orientations with *c*-axes approximately normal to the surface of *Rothpletzella* filaments. However, the nearly random distributions of misorientation axes indicate that individual crystals are not ordered with respect to each other.

These observations can be interpreted as the result of a limited control over mineral formation, resulting either from biologically induced mineralization or entirely abiotic precipitation, e.g., in the presence of the decaying remnants of the organism. The former possibility is in agreement with previous interpretations that *Rothpletzella* might be a colony-forming cyanobacterium. Its morphology and wall structure are similar to those of *Plectonema*, which in turn is considered as a probable extant analog of *Girvanella* (Riding, 1977a; Liu et al., 2016).

Allonema

The crystal organization in shells secreted by metazoans such as brachiopods (England et al., 2007; Pérez-Huerta et al., 2007; Schmahl et al., 2012), bivalves (England et al., 2007), gastropods (Pérez-Huerta et al., 2011), or corals (Coronado et al., 2016) is typically more ordered, phylogenetically constrained and less dependent on the environment than in bacteria, reflecting its biologically controlled character. Likewise, the arrangement of crystals within *Allonema* mineralized structures is very well organized, i.e., characterized by a constrained dispersion of *c*-axes on a girdle within pole figures. The preferred misorientation relationship across adjacent crystals with a rotation mainly around the *c*-axis indicates precipitation of parallel crystals with controlled orientation in a highly ordered manner throughout the mineralized structure. A similar crystallographic relationship has been observed in the trilobite shell.

Crystallographic Parameters Potentially Unique to BCM

Even though the mineralized structure of *Allonema* is highly ordered, no distinct layers or complex crystal morphologies are recognizable. In addition, the *c*-axes are parallel to the elongation of the crystals unlike, e.g., in molluscs or brachiopods. Thus, the crystal structure described here in *Allonema* does not match the parameters of a mineralized structure of any organism known to us. However, only a small number of studies addressing predominantly molluscs are available so far and they also show a great variety of structures. It has been previously shown that highly organized, even hierarchical, crystalline structures are present in stromatolites (Benzerara et al., 2010) and can be produced abiotically in the presence of suitable organic matrices (e.g., Gower and Tirrell, 1998; Nindiyasari et al., 2014, 2015; see also a review by Meldrum, 2003). The difference to previous studies lies in that we do not compare crystal orientations as such, but the spread of misorientations (misorientation angle and especially misorientation axis) between them. A strong crystallographic relationship between adjacent crystals with misorientation axes clustering around the *c*-axis emerges for *Allonema*. It is a consistent characteristic of biominerals produced *via* BCM, even though the degree of crystallographic misorientation varies between species and types of structures: from only a few degrees in the prismatic layer of gastropods (Suzuki et al., 2010), the fiber bundles in bivalve nacre (Maier et al., 2014), or structural subunits of sea urchin teeth (Griesshaber et al., 2012) to *ca.* 40° in brachiopods (e.g., Cusack et al., 2007). The mechanism controlling the range of misorientations is not understood yet. A functional advantage explaining the distribution of misorientations has been proposed with respect to misorientations ordered around the *a*-axes in octocorals (Floquet and Vielzeuf, 2012; Vielzeuf et al., 2017). Such a distribution would allow the *c*-axes of individual crystallites to grow perpendicularly to the growth front even on curved and corrugated surfaces. Based on observations of nacre crystals in red abalone, Gilbert et al. (2008) and Coppersmith et al. (2009) proposed that the limitation of misorientations could be explained by a model of crystal growth kinetics which predicts that the growth of oriented crystals would be faster than that of misoriented ones. This is supported by these authors' observation that the degree of ordering increases gradually with the distance from the nacre-prismatic boundary.

In biomimetic calcite crystals grown in gels, Nindiyasari et al. (2014, 2015) identified experimentally growth conditions affecting the distribution of misorientations at several scales of organization, including misorientations between individual crystallites in mesocrystals and misorientations between mesocrystals. The latter is the scale addressed in our study. The spread of misorientations is highly sensitive to the amount of biopolymers acting as a scaffold during nanocrystal formations (Nindiyasari et al., 2014) and to the presence of additional ions in the medium (Nindiyasari et al., 2015). These experiments may elucidate the mechanism driving the distribution of misorientations *in vivo*, but, similarly as most other published studies so far, cannot be directly compared with our observations, because they do not address the distribution of misorientation axes.

Maier et al. (2014) concluded that biological control over the crystallographic texture is reflected in the frequency distribution of misorientation angles (i.e., log-normal distribution). In contrast, our data reveals an asymmetric bimodal distribution for *Rothpletzella* and trapezoid-shaped distributions for *Allonema* and the trilobite fragments, which would imply a less orderly overall structure. This is in agreement with studies on a range of biomineralizing animals, which show various, but always strictly constrained, distributions of misorientations (e.g., Floquet and Vielzeuf, 2011). In view of the proposed mechanisms and the scarce number of studies available so far, it emerges that perhaps more than one type of frequency distributions of misorientation angles can be characteristic for BCM. However, we observed strong relationships between the orientation of misorientation axes plotted as inverse pole figures and the crystal coordinate system. Thus, we propose the ordering of crystals within a mineralized structure, derived from the distribution patterns of misorientation axes, to be of essential importance for interpretations on the mode of biomineralization.

The occurrence of a strong crystallographic misorientation relationship between adjacent crystals holds not only for metazoans, but—as shown recently—also for sponges (Rossi et al., 2016) and coccolithophores (Hoffmann et al., 2014), suggesting that it may be a universal property of BCM products across all eukaryotes. Nonetheless, for many groups outside Mollusca, EBSD characterization of calcareous structures are still missing or are insufficient to evaluate them using the criterion proposed here (e.g., in serpulids, Chan et al., 2015). In particular, we are not aware of studies of foraminiferal tests which

would document the distribution of misorientations between adjacent crystals. A foraminiferal affinity has been discussed for *Allonema* and similar microproblematica (Wood, 1948; Dzik, 1975; Jarochowska and Munnecke, 2014) and it remains to be tested whether this group provides the most fitting model for the crystallographic properties of *Allonema* mineralized structures.

Limitations of the Study

Our study puts forward a hypothesis on how BCM productsare crystallographically distinct from structures produced *via* BIM, such as those formed by cyanobacteria, and ordered abiotic calcitic structures. Yet an EBSD study of extant cyanobacterial precipitates is missing so far and our hypothesis remains to be tested.

Inability to Distinguish Between BIM and Abiotically Produced Structures

Secondly, to our knowledge, there is so far no criterion allowing to distinguish BIM occurring *in vivo* from mineralization induced on decaying biological remnants, which are abundant in marine sediments, and from abiotic organic polymers (e.g., Gower and Tirrell, 1998; Oppenheimer-Shaanan et al., 2016). Calcification in cyanobacteria is not necessarily an *in vivo* process and may continue after the death of the colony, straddling the boundary with post-mortem cementation and early diagenesis (Bosak and Newman, 2003). Consequently, we cannot be sure that structures observed in lithified samples are associated with the metabolic activity of a cyanobacterium or cements nucleated on its surface. Richter et al. (2008) proposed a criterion according to which BIM would be distinguished from abiotic precipitates by a higher variability (independence) of the crystallographic c-axis with respect to the morphological orientation of the crystal. The authors used this criterion to identify microbially precipitated fibrous calcite-dominated cave deposits, but the findings of clusters of crystals with the same crystallographic orientations within stromatolites (Benzerara et al., 2010) demonstrates that this may not be a universal approach. A wider survey of crystallographic structures of problematic carbonate precipitates is not available yet. In our study, both the putative cyanobacterium Rothpletzella and the non-microbial organism Allonema had c-axes parallel to the elongation of their wall crystals.

Diagenesis

Our study focussed on constraining the mode of (bio)mineralization in problematic fossil structures. This research problem is further complicated by the instability of aragonite, which dissolves during early stages of marine diagenesis (Walter et al., 1993). The voids thus produced are characteristically replaced by early diagenetic cements consisting of equant calcite crystals nucleated on the walls of the voids and often adopting their crystallographic orientations (cements filling the vesicles on **Figures 2**, **3**). More complex diagenetic products emerge in structures composed of a mixture of aragonite and calcite (e.g., Balthasar et al., 2011). Thus, diagenetic recrystallization needs to be taken into account when interpreting EBSD results in fossils. In the case of *Allonema*, the mineralized structure retains its crystalline character even when it is preserved in calcareous claystones which otherwise lack any cements whatsoever (Jarochowska and Munnecke, 2014; Jarochowska et al., 2016). Abiotic crystallization on an organic substrate can be excluded as in all cases the crystalline structure builds a biological structure with complex morphology and even interactions between individuals (Wilson and Taylor, 2014; Jarochowska et al., 2016). The consistency with which the mineralized structure is preserved across depositional and diagenetic environments suggests that it is produced *in vivo* and that *c*-axes parallel to their elongation, visible in fossil specimens, are representative of the original biological structure. With respect to *Rothpletzella*, its walls are microcrystalline, whereas the cements visible between them (**Figure 3**), as well as primarily aragonitic components such as gastropods in the same samples, are replaced with coarse equant cement. But more importantly, carbonate precipitates in cyanobacteria and various groups of algae have been shown experimentally to change the dominant polymorph in function of the seawater composition (Ries et al., 2008). Secular changes in seawater chemistry throughout the Phanerozoic periodically favored either calcite or aragonite precipitates (Sandberg, 1983; Hardie, 1996). BIM products have been predicted to follow this trend closely and indeed the occurrence of microbial calcareous products in the fossil record confirm this prediction (Arp et al., 2001). Samples used here were deposited in a "calcite sea" (Sandberg, 1983; Hardie, 1996), therefore *Rothpletzella* would have to show a substantial control over its biomineralization to counteract kinetically favored calcite precipitation and build an aragonitic skeleton. Altogether, both the type of preservation and the geological context provide important arguments against our specimens being recrystallized. Nonetheless, this question needs to be always considered individually when studying fossil mineralized structures.

CONCLUSIONS

1. Based on a comparison of calcareous mineralized structures of two fossil microproblematica and a fossil metazoan (trilobite), we put forward a hypothesis that the spread of crystallographic misorientations (misorientation angles and misorientation axes) between neighboring grains can serve as a proxy to constrain the degree of control during biomineralization. In particular, constrained and consistent distributions of misorientations can be used to identify biologically controlled biomineralization (BCM). This approach is particularly useful for fossil problematic organisms, which are often attributed to cyanobacteria based on the limited evidence of their simple morphology.
2. EBSD analyses of the fossil microproblematicum *Allonema* reveal elongated granular and acicular crystals with *c*-axes parallel to the elongation and perpendicular to the surface of the organism. The misorientation axes between adjacent crystals are (sub-)parallel to the crystallographic *c*-axis <0001> with a small degree of variation (up to 30°). These observations are interpreted as an orderly and regularly

organized crystal arrangement of the mineralized structure, so far described only from eukaryotes. Therefore, *Allonema* is interpreted to produce its shell *via* BCM.

3. A cyanobacterial affinity is here rejected for *Allonema* since a comparable well-developed crystal organization of the extracellular mineralized structures is not known from cyanobacteria so far. Otherwise the affinity of this problematicum could not be further constrained as for many groups of shell-producing organisms EBSD studies are lacking. The lack of known comparable structures and a consistent fossil record of morphologically similar "ascodictyids" suggest that *Allonema* and potentially other Palaeozoic "pseudobryozoans" might belong to an extinct lineage. It remains to be established whether they were metazoans or belonged to one of the "protest" supergroups.
4. The tube diameter, crystal sizes, and a radial crystal arrangement of the calcareous wall structure of *Rothpletzella* reveal many similarities to fossil and extant cyanobacteria (e.g., *Plectonema*). EBSD analysis revealed a weak organization of the crystal arrangements resulting in a nearly random distribution of misorientation axes. This poor crystal ordering is not typical of BCM and supports the previously proposed cyanobacterial affinity of *Rothpletzella*. However, it was not possible to distinguish whether *Rothpletzella* is produced *via* biologically induced biomineralization (*in vivo*) or *via* abiotic precipitation on an organic matrix.
5. Problematic organisms are common in the Earth history and often play important roles in fossil ecosystems. In case of simple morphologies, the affinity of these organisms may not be possible to constrain. We propose that the integration of morphological and EBSD analysis may help in the determination of the affinity of problematic microfossils based on the crystallographic parameters of their skeletons.

AUTHOR CONTRIBUTIONS

EJ, MB and AM conceived the study. J-FP and MB acquired and analyzed the data, J-FP, EJ, MB, and AM interpreted the results and wrote the manuscript.

FUNDING

The study was supported by funding from the Emerging Talents Initiative of Friedrich-Alexander-Universität Erlangen-Nürnberg to EJ (project no. SS16_Nat_06). We acknowledge support by Deutsche Forschungsgemeinschaft and Friedrich-Alexander-Universität Erlangen-Nürnberg (FAU) within the funding programme Open Access Publishing.

ACKNOWLEDGMENTS

We thank C. Schulbert for assistance with SEM, F. Urban and B. Leipner-Mata for help with sample preparation and I. Oswald for providing samples from Nors. We thank two reviewers and the editor K. Benzerara for suggestions which substantially improved the previous version of the manuscript.

REFERENCES

Altermann, W., Kazmierczak, J., Oren, A., and Wright, D. T. (2006). Cyanobacterial calcification and its rock-building potential during 3.5 billion years of Earth history. *Geobiology* 4, 147–166. doi: 10.1111/j.1472-4669.2006.00076.x

Arp, G., Reimer, A., and Reitner, J. (2001). Photosynthesis-induced biofilm calcification and calcium concentrations in phanerozoic oceans. *Science* 292, 1701–1704. doi: 10.1126/science.1057204

Balthasar, U., Cusack, M., Faryma, L., Chung, P., Holmer, L. E., Jin, J., et al. (2011). Relic aragonite from Ordovician–Silurian brachiopods: implications for the evolution of calcification. *Geology* 39, 967–970. doi: 10.1130/G32269.1

Banfield, J. F., and Hamers, R. J. (1997). Processes at minerals and surfaces with relevance to microorganisms and prebiotic synthesis. *Rev. Mineral. Geochem.* 35, 81–122.

Bazylinski, D. A., and Frankel, R. B. (2003). Biologically controlled mineralization in prokaryotes. *Rev. Mineral. Geochem.* 54, 217–247. doi: 10.2113/0540217

Benzerara, K., Meibom, A., Gautier, Q., Kazmierczak, J., Stolarski, J., Menguy, N., et al. (2010). "Nanotextures of aragonite in stromatolites from the quasi-marine satonda crater lake, Indonesia," in *Tufas and Speleothems: Unravelling the Microbial and Physical Controls,* eds H. M. Pedley, M. Rogerson (London: Geological Society), 211–224. doi: 10.1144/SP336.10

Bestmann, M., and Prior, D. J. (2003). Intragranular dynamic recrystallization in naturally deformed calcite marble: diffusion accommodated grain boundary sliding as a result of subgrain rotation recrystallization. *J. Struct. Geol.* 25, 1597–1613. doi: 10.1016/S0191-8141(03)00006-3

Bosak, T., and Newman, D. K. (2003). Microbial nucleation of calcium carbonate in the Precambrian. *Geology* 31, 577–580. doi: 10.1130/0091-7613(2003)031<0577:MNOCCI>2.0.CO;2

Bosak, T., Souza-Egipsy, V., and Newman, D. K. (2004). A laboratory model of abiotic peloid formation. *Geobiology* 2, 189–198. doi: 10.1111/j.1472-4677.2004.00031.x

Buczynski, C., and Chafetz, H. S. (1993). "Habit of bacterially induced precipitates of calcium carbonate: examples from laboratory experiments and recent sediments," in *Carbonate Microfabrics,* eds R. Rezak and D. L. Lavoie (New York, NY: Springer-Verlag), 105–116.

Chan, V. B. S., Toyofuku, T., Wetzel, G., Saraf, L., Thiyagarajan, V., and Mount, A. S. (2015). Direct deposition of crystalline aragonite in the controlled biomineralization of the calcareous tubeworm. *Front. Mar. Sci.* 2:97. doi: 10.3389/fmars.2015.00097

Coppersmith, S. N., Gilbert, P. U. P. A., and Metzler, R. A. (2009). Theoretical characterization of a model of aragonite crystal orientation in red abalone nacre. *J. Phys. A Math. Theor.* 42:125101. doi: 10.1088/1751-8113/42/12/125101

Coronado, I., Pérez-Huerta, A., and Rodríguez, S. (2016). Analogous biomineralization processes between the fossil coral *Calceola sandalina* (Rugosa, Devonian) and other Recent and fossil cnidarians. *J. Struct. Biol.* 196, 173–186. doi: 10.1016/j.jsb.2016.06.013

Cusack, M. (2016). Biomineral electron backscatter diffraction for palaeontology. *Palaeontology* 59, 171–179. doi: 10.1111/pala.12222

Cusack, M., Pérez-Huerta, A., and Dalbeck, P. (2007). Common crystallographic control in calcite biomineralization of bivalved shells. *CrystEngComm* 9, 1215–1218. doi: 10.1039/B708795K

Dzik, J. (1975). The origin and early phylogeny of the cheilostomatous bryozoa. *Acta Palaeontol. Pol.* 20, 395–423.

England, J., Cusack, M., Dalbeck, P., and Pérez-Huerta, A. (2007). Comparison of the crystallographic structure of semi nacre and nacre by electron backscatter diffraction. *Cryst. Growth Des.* 7, 307–310. doi: 10.1021/cg060374p

Floquet, N., and Vielzeuf, D. (2011). Mesoscale twinning and crystallographic registers in biominerals. *Am. Mineral.* 96, 1228–1237. doi: 10.2138/am.2011.3805

Floquet, N., and Vielzeuf, D. (2012). Ordered misorientations and preferential directions of growth in mesocrystalline red coral sclerites. *Cryst. Growth Des.* 12, 4805–4820. doi: 10.1021/cg300528h

Flügel, E. (ed.). (2004). "Cyanobacteria and calcimicrobes," in *Microfacies of Carbonate Rocks. Analysis, Interpretation and Application* (Berlin: Springer), 408–412.

Frankel, R. B., and Bazylinski, D. A. (2003). Biologically induced mineralization by bacteria. *Rev. Mineral. Geochem.* 54, 95–114. doi: 10.2113/0540095

Gilbert, P. U. P. A., Metzler, R. A., Zhou, D., Scholl, A., Doran, A., Young, A., et al. (2008). Gradual ordering in red abalone nacre. *J. Am. Chem. Soc.* 130, 17519–17527. doi: 10.1021/ja8065495

Gower, L. A., and Tirrell, D. A. (1998). Calcium carbonate films and helices grown in solutions of poly(aspartate). *J. Cryst. Growth* 191, 153–160. doi: 10.1016/S0022-0248(98)00002-5

Griesshaber, E., Goetz, A. J., Howard, L., Ball, A., Ruff, S., and Schmahl, W. W. (2012). Crystal architecture of the tooth and jaw bone (pyramid) of the sea urchin Paracentrotus lividus. *Bioinspired Biomim. Nanobiomat.* 1, 133–139. doi: 10.1680/bbn.11.00018

Griesshaber, E., Neuser, R. D., and Schmahl, W. W. (2010). The application of EBSD analysis to biomaterials: microstructural and crystallographic texture variations in marine carbonate shells. *Semin. Soc. Esp. Mineral.* 7, 22–34.

Hardie, L. A. (1996). Secular variation in seawater chemistry: an explanation for the coupled secular variation in the mineralogies of marine limestones and potash evaporites over the past 600 m.y. *Geology* 24, 279–283. doi: 10.1130/0091-7613(1996)024<0279:SVISCA>2.3.CO;2

Hoffmann, R., Wochnik, A. S., Heinzl, C., Betzler, S. B., Matich, S., Griesshaber, E., et al. (2014). Nanoprobe crystallographic orientation studies of isolated shield elements of the coccolithophore species *Emiliania huxleyi*. *Eur. J. Mineral.* 26, 473–483. doi: 10.1127/0935-1221/2014/0026-2365

Jarochowska, E., Hierl, F., Vinn, O., and Munnecke, A. (2016). Reducing taxonomic noise in problematic fossils: revision of the incertae sedis genus *Allonema* based on shape analysis. *Bull. Geosci.* 91, 97–110. doi: 10.3140/bull.geosci.1588

Jarochowska, E., and Munnecke, A. (2014). The Paleozoic problematica *Wetheredella* and *Allonema* are two aspects of the same organism. *Facies* 60, 651–662. doi: 10.1007/s10347-014-0399-z

Kazmierczak, J., and Altermann, W. (2002). Neoarchean biomineralization by benthic cyanobacteria. *Science* 298, 2351–2351. doi: 10.1126/science.1075933

Knoll, A. H. (2003). Biomineralization and evolutionary history. *Rev. Mineral. Geochem.* 54, 329–356. doi: 10.2113/0540329

Liu, L., Wu, Y., Yang, H., and Riding, R. (2016). Ordovician calcified cyanobacteria and associated microfossils from the Tarim Basin, Northwest China: systematics and significance. *J. Syst. Palaeontol.* 14, 183–210. doi: 10.1080/14772019.2015.1030128

Lochte, K., and Turley, C. M. (1988). Bacteria and cyanobacteria associated with phytodetritus in the deep sea. *Nature* 333, 67–69. doi: 10.1038/333067a0

Lowenstam, H. (1981). Minerals formed by organisms. *Science* 211, 1126–1131. doi: 10.1126/science.7008198

Lowenstam, H. (1986). "Mineralization processes in monerans and protoctists," in *Biomineralization in Lower Plants and Animals,* eds B. S. C. Leadbeater and R. Riding (Oxford: Oxford University Press), 1–17.

Maier, B. J., Griesshaber, E., Alexa, P., Ziegler, A., Ubhi, H. S., and Schmahl, W. W. (2014). Biological control of crystallographic architecture: hierarchy and co-alignment parameters. *Acta Biomater.* 10, 3866–3874. doi: 10.1016/j.actbio.2014.02.039

Meldrum, F. C. (2003). Calcium carbonate in biomineralisation and biomimetic chemistry. *Int. Mater. Rev.* 48, 187–224. doi: 10.1179/095066003225005836

Merz, M. U. E. (1992). The biology of carbonate precipitation by cyanobacteria. *Facies* 26, 81–101. doi: 10.1007/BF02539795

Nindiyasari, F., Fernández-Díaz, L., Griesshaber, E., Astilleros, J. M., Sánchez-Pastor, N., and Schmahl, W. W. (2014). Influence of gelatin hydrogel porosity on the crystallization of $CaCO_3$. *Cryst. Growth Des.* 14, 1531–1542. doi: 10.1021/cg401056t

Nindiyasari, F., Ziegler, A., Griesshaber, E., Fernández-Díaz, L., Huber, J., Walther, P., et al. (2015). Effect of hydrogel matrices on calcite crystal growth morphology, aggregate formation, and co-orientation in biomimetic experiments and biomineralization environments. *Cryst. Growth Des.* 15, 2667–2685. doi: 10.1021/cg5018483

Nose, M., Schmid, D. U., and Leinfelder, R. R. (2006). Significance of microbialites, calcimicrobes, and calcareous algae in reefal framework formation from the Silurian of Gotland, Sweden. *Sediment. Geol.* 192, 243–265. doi: 10.1016/j.sedgeo.2006.04.009

Obst, M., Wehrli, B., and Dittrich, M. (2009). $CaCO_3$ nucleation by cyanobacteria: laboratory evidence for a passive, surface-induced mechanism. *Geobiology* 7, 324–347. doi: 10.1111/j.1472-4669.2009.00200.x

Oppenheimer-Shaanan, Y., Sibony-Nevo, O., Bloom-Ackermann, Z., Suissa, R., Steinberg, N., Kartvelishvily, E., et al. (2016). Spatio-temporal assembly of functional mineral scaffolds within microbial biofilms. *NPJ Biofilms Microbiomes* 2:15031. doi: 10.1038/npjbiofilms.2015.31

Pérez-Huerta, A., Cusack, M., and England, J. (2007). Crystallography and diagenesis in fossil craniid brachiopods. *Palaeontology* 50, 757–763. doi: 10.1111/j.1475-4983.2007.00688.x

Pérez-Huerta, A., Dauphin, Y., Cuif, J. P., and Cusack, M. (2011). High resolution electron backscatter diffraction (EBSD) data from calcite biominerals in recent gastropod shells. *Micron* 42, 246–251. doi: 10.1016/j.micron.2010.11.003

Planavsky, N., Reid, R. P., Lyons, T. W., Myshrall, K. L., and Visscher, P. T. (2009). Formation and diagenesis of modern marine calcified cyanobacteria. *Geobiology* 7, 566–576. doi: 10.1111/j.1472-4669.2009.00216.x

Prior, D. J., Boyle, A. P., Brenker, F., Cheadle, M. C., Day, A., Lopez, G., et al. (1999). The application of electron backscatter diffraction and orientation contrast imaging in the SEM to textural problems in rocks. *Am. Mineral.* 84, 1741–1759. doi: 10.2138/am-1999-11-1204

Prior, D. J., Wheeler, J., Peruzzo, L., Spess, R., and Storey, C. (2002). Some garnet microstructures: an illustration of the potential of orientation maps and misorientation analysis in microstructural studies. *J. Struct. Geol.* 24, 999–1011. doi: 10.1016/S0191-8141(01)00087-6

Richter, D. K., Immenhauser, A., and Neuser, R. D. (2008). Electron backscatter diffraction documents randomly orientated c-axes in moonmilk calcite fibres: evidence for biologically induced precipitation. *Sedimentology* 55, 487–497. doi: 10.1111/j.1365-3091.2007.00915.x

Riding, R. (1977a). Calcified *Plectonema* (blue-green algae), a recent example of *Girvanella* from Aldabra Atoll. *Palaeontology* 20, 33–46.

Riding, R. (1977b). Systematics of *Wetheredella*. *Lethaia* 10, 94–94. doi: 10.1111/j.1502-3931.1977.tb00596.x

Riding, R. (1991). "Calcified cyanobacteria," in *Calcareous Algae and Stromatolites,* ed R. Riding (Berlin: Springer), 55–87.

Riding, R. (2006). Cyanobacterial calcification, carbon dioxide concentrating mechanisms, and Proterozoic–Cambrian changes in atmospheric composition. *Geobiology* 4, 299–316. doi: 10.1111/j.1472-4669.2006.00087.x

Riding, R. (2011). "Calcified cyanobacteria," in *Encyclopedia of Geobiology*, eds J. Reitner and V. Thiel (Heidelberg: Springer), 211–223.

Riding, R., and Voronova, L. (1984). Assemblages of calcareous algae near the precambrian/cambrian boundary in siberia and mongolia. *Geol. Mag.* 121, 205–210. doi: 10.1017/S0016756800028260

Ries, J. B., Anderson, M. A., and Hill, R. T. (2008). Seawater Mg/Ca controls polymorph mineralogy of microbial $CaCO_3$: a potential proxy for calcite-aragonite seas in Precambrian time. *Geobiology* 6, 106–119. doi: 10.1111/j.1472-4669.2007.00134.x

Rossi, A. L., Ribeiro, B., Lemos, M., Werckmann, J., Borojevic, R., Fromont, J., et al. (2016). Crystallographic orientation and concentric layers in spicules of calcareous sponges. *J. Struct. Biol.* 196, 164–172. doi: 10.1016/j.jsb.2016.04.009

Sandberg, P. A. (1983). An oscillating trend in Phanerozoic non-skeletal carbonate mineralogy. *Nature* 305:19. doi: 10.1038/305019a0

Schmahl, W. W., Griesshaber, E., Kelm, K., Goetz, A., Jordan, G., Ball, A., et al. (2012). Hierarchical structure of marine shell biomaterials: biomechanical functionalization of calcite by brachiopods. *Zeitschr. Kristallogr.* 227, 793–804. doi: 10.1524/zkri.2012.1542

Schopf, J., and Packer, B. (1987). Early Archean (3.3-billion to 3.5-billion-year-old) microfossils from Warrawoona group, Australia. *Science* 237, 70–73. doi: 10.1126/science.11539686

Shen, Y., and Neuweiler, F. (2016). Taphocoenoses and diversification patterns of calcimicrobes and calcareous algae, Ordovician, Tarim Basin, China. *Can. J. Earth Sci.* 53, 702–711. doi: 10.1139/cjes-2015-0173

Suzuki, M., Kameda, J., Sasaki, T., Saruwatari, K., Nagasawa, H., and Kogure, T. (2010). Characterization of the multilayered shell of a limpet, *Lottia kogamogai* (Mollusca: patellogastropoda), using SEM–EBSD and FIB–TEM techniques. *J. Struct. Biol.* 171, 223–230. doi: 10.1016/j.jsb.2010.04.008

Swett, K., and Knoll, A. H. (1985). Stromatolitic bioherms and microphytolites from the late proterozoic draken conglomerate formation, spitsbergen. *Precambrian Res.* 28, 327–347. doi: 10.1016/0301-9268(85)90037-3

Ulrich, E. O., and Bassler, R. S. (1904). A revision of the Paleozoic bryozoa, part i: on genera and species of Ctenostomata. *Smithson. Miscellaneous Collect.* 45, 256–294.

Vachard, D., and Cózar, P. (2010). An attempt of classification of the Palaeozoic *incertae sedis* Algospongia. *Rev. Español. Micropaleonto.* 42, 129–241.

Van Cappellen, P. (2003). Biomineralization and global biogeochemical cycles. *Rev. Mineral. Geochem.* 54, 357–381. doi: 10.2113/0540357

Vielzeuf, D., Floquet, N., Perrin, J., Tambutté, E., and Ricolleau, A. (2017). Crystallography of complex forms: the case of octocoral sclerites. *Cryst. Growth Des.* 17, 5080–5097. doi: 10.1021/acs.cgd.7b00087

Walter, L. M., Bischof, S. A., Patterson, W. P., Lyons, T. W., O'nions, R. K., Gruszczynski, M., et al. (1993). Dissolution and recrystallization in modern shelf carbonates: evidence from pore water and solid phase chemistry [and discussion]. *Philos. Trans.* 344, 27–36. doi: 10.1098/rsta.1993.0072

Weiner, S., and Dove, P. M. (2003). An overview of biomineralization processes and the problem of the vital effect. *Rev. Mineral. Geochem.* 54, 1–29. doi: 10.2113/0540001

Wheeler, J., Prior, D. J., Jiang, Z., Spiess, R., and Trimby, P. W. (2001). The petrological significance of misorientations between grains. *Contrib. Mineral. Petrol.* 141, 109–124. doi: 10.1007/s004100000225

Wilson, M. A., and Taylor, P. D. (2001). "Pseudobryozoans" and the problem of encruster diversity in the Paleozoic. *PaleoBios* 21, 134–135.

Wilson, M. A., and Taylor, P. D. (2014). The morphology and affinities of *Allonema* and *Ascodictyon*, two abundant Palaeozoic encrusters commonly misattributed to the ctenostome bryozoans. *Stud. Trent. Sci. Nat.* 94, 259–266.

Wood, A. (1948). "*Sphaerocodium*," a misinterpreted fossil from the Wenlock limestone. *Proc. Geol. Assoc.* 59, 9–22. doi: 10.1016/S0016-7878(48)80027-1

Wray, J. L. (1977). *Calcareous Algae*. Amsterdam: Elsevier.

Zhang, Y., Li, Y., Wang, G., and Munnecke, A. (2017). Windward and leeward margins of an Upper Ordovician carbonate platform in the Central Tarim Uplift, Xinjiang, northwestern China. *Palaeogeogr. Palaeoclimatol. Palaeoecol.* 474, 79–88. doi: 10.1016/j.palaeo.2016.12.040

Conflict of Interest Statement: The authors declare that the research was conducted in the absence of any commercial or financial relationships that could be construed as a potential conflict of interest.